

Ideal orientations and persistence characteristics of hexagonal close packed crystals in simple shear

Benoît Beausir^{a,b}, László S. Tóth^{b,*}, Kenneth W. Neale^a

^a Faculty of Engineering, Université de Sherbrooke, Sherbrooke, Que., Canada J1K 2R1

^b Laboratoire de Physique et Mécanique des Matériaux, Université de Metz, Ile du Saulcy, 57045 Metz, France

Received 25 October 2006; received in revised form 30 November 2006; accepted 2 December 2006

Available online 20 February 2007

Abstract

The ideal positions and fibres of hexagonal close packed (hcp) crystals subjected to simple shear are explored in orientation space for the first time using the viscoplastic full constraints crystal plasticity approach with the help of an orientation persistence factor developed earlier for face-centred cubic crystals. Five ideal fibres are identified; these are named B, P, Y and C₁–C₂, and correspond to a high activity of $\langle a \rangle$ type slip (B, P and Y) as well as pyramidal $\langle c + a \rangle$ (C₁–C₂). Although the numerical examples are given for the case of magnesium, the main features are the same for other hcp crystals. The characteristics of the three-dimensional lattice rotation fields are also investigated in Euler space. It has been found that the rotation field is asymmetric around the ideal fibres: convergent on one side and divergent on the other. The main drift of orientations is in the direction of the material spin. Some simulation results obtained with the Taylor viscoplastic polycrystal code for simple shear of magnesium are interpreted with the help of the persistence characteristics of the rotation field.

© 2007 Acta Materialia Inc. Published by Elsevier Ltd. All rights reserved.

Keywords: Simple shear; Magnesium; Ideal positions; Stability; Textures

1. Introduction

Metals with hexagonal crystal structure (e.g. titanium alloys, magnesium alloys, beryllium and zirconium) are now the focus of interest for technical applications and academic research. Depending on their properties, these metals are used in very different applications (aeronautic, transport, nuclear). Their mechanical properties have been extensively studied to determine the possibilities and limits of shape forming. Large plastic strains, however, involve the development of plastic anisotropy which can be especially strong in hexagonal close packed (hcp) polycrystals. This is why it is important to know the ideal crystallographic textures that develop at large strains. These textures have been studied intensively for compression, tension, plane strain compression and rolling. They are

not known, however, under simple shear or torsion conditions. The aim of the present work is to determine the ideal texture components that develop during simple shear of hcp polycrystals and examine their persistence characteristics in orientation space.

The technique employed in the present work is similar to the one proposed by Tóth et al. [1] for the face centred cubic (fcc) case. It is based on the lattice spin $\underline{\underline{\Omega}}$ which is calculated from a crystal plasticity model. From $\underline{\underline{\Omega}}$, a so-called persistence parameter is defined

$$P(\mathbf{g}, \dot{\underline{\underline{\varepsilon}}}) = \ln \frac{1}{|\underline{\underline{\Omega}}(\mathbf{g}, \dot{\underline{\underline{\varepsilon}}})|/\bar{\dot{\varepsilon}}}, \quad (1)$$

where \mathbf{g} denotes the orientation $\mathbf{g} = (\varphi_1, \varphi, \varphi_2)$ (here \mathbf{g} is a vector quantity with $\varphi_1, \varphi, \varphi_2$ being the three Euler angles [2]), $\dot{\underline{\underline{\varepsilon}}}$ is the strain rate tensor and $\bar{\dot{\varepsilon}}$ is the applied von Mises equivalent strain rate. When the lattice spin is small, i.e. when grain rotation is small, P is high (characteristic of an ideal orientation). This parameter proved to be very use-

* Corresponding author. Tel.: +33 387547238; fax: +33 387315366.
E-mail address: toth@univ-metz.fr (L.S. Tóth).

ful in the determination of the ideal stable components of the crystallographic texture [3–8]. Nevertheless, for a complete understanding of the evolution of the texture, one has to examine also the velocity rotation field $\dot{\mathbf{g}} = (\dot{\varphi}_1, \dot{\varphi}, \dot{\varphi}_2)$ as well as the divergence quantity throughout the entire orientation space. The latter is defined by

$$\text{div}(\dot{\mathbf{g}}) = \frac{\partial \dot{\varphi}_1}{\partial \varphi_1} + \frac{\partial \dot{\varphi}}{\partial \varphi} + \frac{\partial \dot{\varphi}_2}{\partial \varphi_2}. \quad (2)$$

Several such studies have been carried out in which the rotation field has been examined [1,3–8]. One of the most interesting features found about the rotation field in Euler space under simple shear of fcc and body centred cubic (bcc) crystals is that, for all ideal orientations, $\text{div}(\dot{\mathbf{g}}) = 0$, i.e. the ideal fibres are situated between the positive and negative regions of the divergence [4,7]. This particularity of the rotation field distinguishes the simple shear deformation mode from other deformations (e.g. rolling, compression or tension) and readily explains the observed texture variations in fcc and bcc materials. One of the purposes of the present work is to find out similar features for the hexagonal case.

Hexagonal crystals have fewer symmetries than cubic; only a sixfold symmetry around their c -axis in contrast to 24 in cubic. Another difference is the operating slip systems, which can be grouped into families. These slip systems are basal $\{0001\}\langle 1\bar{2}10 \rangle$, prismatic $\{1\bar{1}00\}\langle 11\bar{2}0 \rangle$, pyramidal $\langle a \rangle \{10\bar{1}1\}\langle \bar{1}2\bar{1}0 \rangle$, pyramidal $\langle c+a \rangle$ type A $\{10\bar{1}1\}\langle 2\bar{1}\bar{1}\bar{3} \rangle$ and pyramidal $\langle c+a \rangle$ type B $\{2\bar{1}\bar{1}2\}\langle 2\bar{1}13 \rangle$. Their activity depends mostly on the c/a ratio of the unit cell. Usually, more than one slip system family needs to be activated because there are families that contain less than five independent slip systems (i.e. basal and prismatic), which is the minimum number to accommodate a general prescribed deformation. The critical resolved shear stresses (crss) at which they are activated are not always known. They can be obtained by experiments on single crystals [9,10] or by simulating the evolution of the texture [11–16].

In the present work, we consider the case of magnesium, for different sets of relative crss values (in this work, because of viscoplastic slip, crss means the reference stress, not the critical resolved shear stress, as defined in Eq. (4) below). The results obtained will also be qualitatively valid for other hcp structures; nevertheless, for exact results, the analyses should be repeated. First the ideal orientations will be determined by an analysis of the persistence parameter in Euler space, and then the rotation field together with the divergence will be examined. Finally, simulations will be performed for torsion of magnesium in comparison with experiments using the Taylor viscoplastic polycrystal model.

2. Fundamental relations

A simple shear loading is imposed on the hexagonal structure defined by the following constant velocity gradient:

$$\underline{\underline{L}} = \dot{\gamma} \begin{pmatrix} 0 & 1 & 0 \\ 0 & 0 & 0 \\ 0 & 0 & 0 \end{pmatrix}. \quad (3)$$

In order to obtain a von-Mises equivalent strain rate of 1.0 s^{-1} , the value of $\dot{\gamma}$ was $\sqrt{3} \text{ s}^{-1}$ in the calculations. In the following, our orientation stability analysis is restricted to the Taylor model for which $\underline{\underline{L}}$ is the same for any grain.

In the orientation stability study, the full constraints viscoplastic crystal plasticity model was employed with rate-dependent plastic slip of the form [17]

$$\tau^{s,f} = \tau_0^f \text{sgn}(\dot{\gamma}^{s,f}) \left| \frac{\dot{\gamma}^{s,f}}{\dot{\gamma}_0} \right|^m = \tau_0^f \frac{\dot{\gamma}^{s,f}}{\dot{\gamma}_0} \left| \frac{\dot{\gamma}^{s,f}}{\dot{\gamma}_0} \right|^{m-1}. \quad (4)$$

Here $\tau^{s,f}$ is the resolved shear stress in the slip system indexed by s of the family indexed by f , $\dot{\gamma}^{s,f}$ is the slip rate, the τ_0^f value is the reference stress level (at which the slip rate is $\dot{\gamma}_0$), and m is the strain rate sensitivity index. The reference shear rate $\dot{\gamma}_0$ is supposed to be the same for all slip systems. Eq. (4) has been widely used in crystal plasticity simulations (e.g. [1,3–8,11–21]). The slip systems are grouped into “families” for which purpose the index f is used. The main families in hexagonal structures are the basal, prismatic and pyramidal slips. It is assumed here that the reference shear stress τ_0^f is the same within a given slip system family, but can differ from one family to another. The behaviour of hcp metals is strongly dependent on the values of the reference shear stresses τ_0^f and on m . In the present investigation, several sets of reference shear stresses and of strain rate sensitivity index m are considered. Hereafter, the reference stresses of the slip system families will be referred in the following order: $[\tau_0^{\text{basal}}, \tau_0^{\text{prism}}, \tau_0^{\text{pyr.}(a)}, \tau_0^{\text{pyr.}(c+a)/A}, \tau_0^{\text{pyr.}(c+a)/B}]$.

In the orientation stability study, it is necessary to distinguish among three types of rotations (elastic distortions are neglected). They are $\underline{\underline{\beta}}$, the material spin, which is the skew-symmetric part of the velocity gradient $\underline{\underline{L}}$ relative to the fixed reference system

$$\beta_{ij} = \frac{L_{ij} - L_{ji}}{2}. \quad (5)$$

$\underline{\underline{\omega}}$, the plastic spin, which is the skew-symmetric part of the velocity gradient corresponding to plastic slip only, with respect to the fixed reference system. It is given by [22,23]

$$\omega_{ij} = \sum_{f=1}^{\text{nf}} \sum_{s=1}^{\text{nsf}} \frac{m_{ij}^{s,f} - m_{ji}^{s,f}}{2} \dot{\gamma}^{s,f}. \quad (6)$$

Finally, the lattice spin $\underline{\underline{\Omega}}$, which is the rate of rotation of the crystallographic directions with respect to the fixed reference system. (The index nf denotes the total number of families and nsf is the number of slip systems in family f .)

The following relation exists between the above-defined spin quantities [24]:

$$\underline{\underline{\Omega}} = \underline{\underline{\beta}} - \underline{\underline{\omega}}. \quad (7)$$

Each orientation \mathbf{g} is defined by the three Euler angles $(\varphi_1, \varphi, \varphi_2)$. Using a crystal plasticity model, the corresponding rotation velocity field $\dot{\mathbf{g}} = (\dot{\varphi}_1, \dot{\varphi}, \dot{\varphi}_2)$ can be calculated for any \mathbf{g} . The components of the velocity $\dot{\mathbf{g}}$ can be obtained as follows [25,26]:

$$\begin{aligned}\dot{\varphi}_1 &= \Omega_{12} - \varphi_2 \cos \varphi, \\ \dot{\varphi} &= \Omega_{32} \cos \varphi_1 + \Omega_{13} \sin \varphi_1, \\ \dot{\varphi}_2 &= (\Omega_{32} \sin \varphi_1 - \Omega_{13} \cos \varphi_1) / \sin \varphi,\end{aligned}\quad (8)$$

where the lattice spin Ω is defined with respect to the sample axes. These relations can be obtained from

$$\underline{\dot{T}} = \underline{\Omega T}, \quad (9)$$

where \underline{T} is the transformation matrix going from the sample to the crystal axes. (The \underline{T} matrix expresses the same transformation as the \mathbf{g} vector, they are, however, mathematically different quantities; this is the reason why the orientation change is calculated from Eq. (9).)

3. Maps of orientation persistence

The stability of an orientation is examined here with the help of the persistence parameter P defined by Eq. (1). In that relation, the norm of the lattice spin is given by

$$|\underline{\Omega}| = (\Omega_{32}^2 + \Omega_{31}^2 + \Omega_{12}^2)^{1/2}. \quad (10)$$

With the help of relations Eq. (8), P can be rewritten as

$$P = \ln \frac{\bar{\varepsilon}}{\sqrt{\dot{\varphi}_1^2 + \dot{\varphi}^2 + \dot{\varphi}_2^2 + 2\dot{\varphi}_1\dot{\varphi}_2 \cos \varphi}}. \quad (11)$$

As can be seen in this relation, P depends on $\cos \varphi$, which is a consequence of the distortion of Euler space in the φ coordinate [27]. $\bar{\varepsilon}$ will be taken as 1.0 s^{-1} in the calculation of P , but actually P is independent of the applied strain rate because the $\dot{\varphi}_1$, $\dot{\varphi}$ and $\dot{\varphi}_2$ quantities are proportional to the magnitude of the applied strain rate. (Only the stress level changes when the strain rate is changed; see Eq. (4).)

For the case of a hexagonal crystal structure and simple shear, the symmetries (sixfold around the c -axis and twofold around the axis defined as normal to the shear axis and the shear plane axis) permit the smallest possible representative Euler space volume to be defined as follows:

$$\varphi_1 = 0 \rightarrow 180^\circ, \quad \varphi = 0 \rightarrow 90^\circ, \quad \varphi_2 = 0 \rightarrow 60^\circ. \quad (12)$$

For the definition of the Euler angles, the Cartesian reference system is fixed to the unit cell of the hexagonal crystal structure so that the axes x_1 , x_2 and x_3 are parallel to the axes $[10\bar{1}0]$, $[\bar{1}2\bar{1}0]$, $[0001]$, respectively. In order to map the P parameter in orientation space, the space defined by Eq. (12) was subdivided into a grid of the size $3^\circ \times 3^\circ \times 3^\circ$. The orientation stability parameter P was calculated using the Taylor model at each grid point (36,000 points for the full representation). P Depends not only on the strain rate sensitivity m but also on the values of the reference stresses τ_0^f .

Fig. 1 shows the isovalue-maps of P in the restrained Euler space for six sets of the relative reference stresses $[1, 30, 30, 30, 30]$ (Fig. 1a), $[30, 1, 30, 30, 30]$ (Fig. 1b), $[30, 30, 1, 30, 30]$ (Fig. 1c), $[30, 30, 30, 1, 30]$ (Fig. 1d), $[30, 30, 30, 30, 1]$ (Fig. 1e), and $[1, 1, 1, 1, 1]$ (Fig. 1f), for a strain rate sensitivity value of $m = 0.2$, which corresponds to a temperature of about 250°C in Mg (an experimentally determined value $m = 0.15$ at 200°C in AZ31 has been reported [14]). The colours indicate the magnitude of P , which is high for red and low for blue. The above selection of the relative reference stress values reveals the existence of five ideal fibres. The skeleton lines of the fibres were traced in orientation space and plotted in the (0002) and $(10\bar{1}0)$ pole figures in Fig. 2. They are named and defined as follows:

1. The B fibre ($0^\circ, 90^\circ, 0\text{--}60^\circ$); basal plane \parallel shear plane.
2. The P fibre ($0^\circ, 0\text{--}90^\circ, 30^\circ$); $\langle a \rangle \parallel$ shear direction. The end-orientation of this fibre is called P_1 , its appearance in the $\varphi = 0^\circ$ section is redundant along several lines for two reasons: (i) because of the singularity of Euler space at $\varphi = 0^\circ$; (ii) it appears also at different locations because of the hexagonal crystal symmetry.
3. The Y fibre ($0^\circ, 30^\circ, 0\text{--}60^\circ$); this is a ‘ c ’ fibre, meaning that the fibre axis is the c -axis which is rotated towards the shear plane by 30° .
- 4–5. The C_1 fibre ($60^\circ, 90^\circ, 0\text{--}60^\circ$) and C_2 fibre ($120^\circ, 90^\circ, 0\text{--}60^\circ$); these are also ‘ c ’ fibres where the c -axis is first rotated 90° in the shear direction, then $\pm 30^\circ$ in the shear plane direction.

The B, C_1 , C_2 and Y fibres appear as simple points in the (0002) pole figure, while the P fibre is a line in both the (0002) and $(10\bar{1}0)$ pole figures. This is a consequence of the perpendicularity of the two pole figure projections.

Note that, because of the sample symmetry corresponding to simple shear, P is the same on the $\varphi_1 = 0^\circ$ and $\varphi_1 = 180^\circ$ planes of Euler space, so fibres P, B and Y are repeated at these locations. Similarly, as a consequence of the hexagonal crystal symmetry, the $\varphi_2 = 0$ and $\varphi_2 = 60^\circ$ planes are identical in orientation space.

The intensity of the orientation stability parameter P is not the same for the different fibres as P depends very much on the relative reference stress values. As an example, Fig. 1f shows a P -map when the reference stresses are all equal to 1.0. For this special case (which is not realistic in hcp materials as well-characterized hcp metals do not have equal critical stresses on the different modes) only three fibres – the B and C_1 – C_2 as well as a single orientation, the P_1 ($30^\circ, 0^\circ, 0^\circ$) – are significant. This case demonstrates the effect of geometrical differences of the slip system families on their activities during simple shear.

The above analysis could be repeated with a more “realistic” combination of the reference stresses τ_0^f . Although the persistence parameter depends quite strongly on the relative strengths of the slip system families, the position of an ideal fibre does not depend on the reference stresses values; it is exclusively determined by the geometry of the crystal,

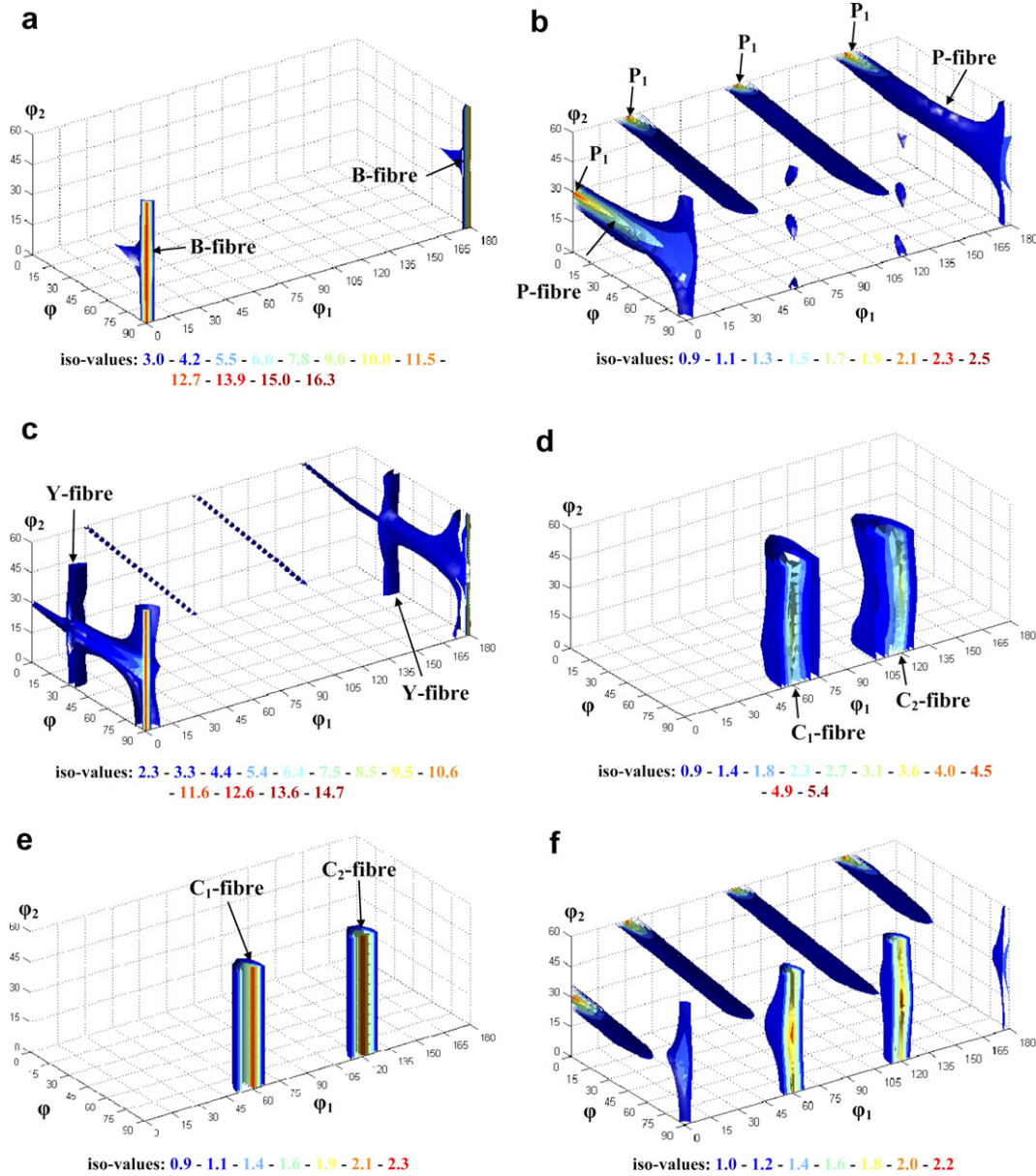


Fig. 1. Isovalues of orientation stability parameter P in the restrained Euler space for the following sets of reference stresses: (a) [1, 30, 30, 30, 30], (b) [30, 1, 30, 30, 30], (c) [30, 30, 1, 30, 30], (d) [30, 30, 30, 1, 30], (e) [30, 30, 30, 30, 1] and (f) [1, 1, 1, 1, 1].

i.e., by the c/a ratio. Nevertheless, the actual combination of the reference stresses depends on the material, so the texture development should depend on the selected combination of the crss values. According to the study of Agnew et al. [14] for magnesium AZ31, the set of [1, 8, 8, 6, 6] gave the best comparison between simulated and experimental textures using the self-consistent viscoplastic model (VPSC).

Fig. 3 presents the ideal positions for the set of reference stresses [1, 8, 8, 6, 6]. Two fibres appear: the B and the P, the latter with low intensity. This case is not far from that presented in Fig. 1a because of the relatively low value of τ_0^{basal} .

For a better comprehension of the contribution of the different slip system families to the stability of the ideal components, the relative activity of the slip system families

is investigated along the fibres. The activity A^f of family f is defined by the ratio of the sum of the absolute value of the slips γ^f of family f with respect to the total glides γ^g in the grain:

$$A^f = \frac{\gamma^f}{\gamma^g} = \frac{\sum_s |\gamma^{s,f}|}{\sum_f \sum_s |\gamma^{s,f}|}. \quad (13)$$

Fig. 4 presents the slip activity A^f by families along the fibres identified above for the set of crss [1, 8, 8, 6, 6] for $m = 0.2$. The pair of fibres C_1 – C_2 is plotted in the same figures as their activity is identical. As can be seen in Fig. 4, only basal slip is activated along the B fibre. For all the other four fibres, all slip system families are active along the fibres. When looking at the slip directions only, one

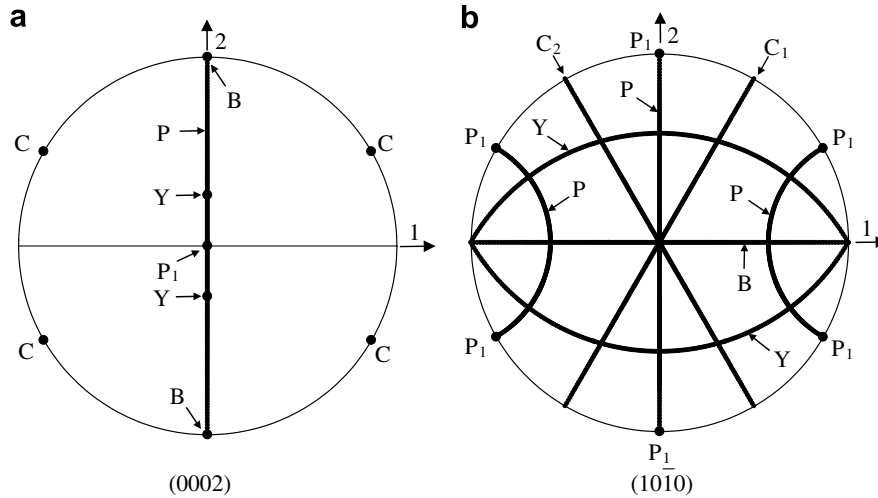


Fig. 2. Ideal orientations of magnesium under simple shear as they appear in the (a) (0002) and (b) (10 $\bar{1}$ 0) pole figures.

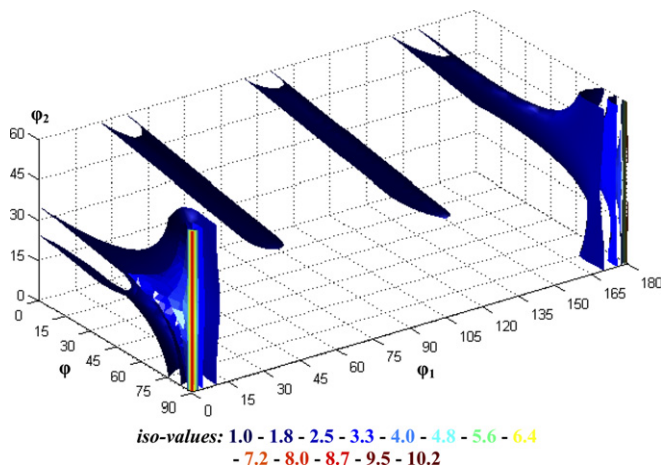


Fig. 3. Map of the orientation stability parameter P in Euler space for Mg using the set of reference stresses [1, 8, 8, 6, 6].

can find out that along the P and Y fibres the most active slip modes involve only $\langle a \rangle$ type dislocations. Along the C_1 – C_2 fibres the most active slip systems produce dislocations with $\langle c + a \rangle$ type Burgers vectors.

The orientation stability parameter P depends not only on the orientation but also on the strain rate sensitivity index m . Fig. 5 shows the evolution of P along all fibres for the set of reference stresses [1, 8, 8, 6, 6] for two values of m : 0.2 (a) and 0.1 (b). As can be seen in Fig. 5, the lower the m , the higher the P value. For example, for the B fibre, the orientation stability parameter P increases 35-fold between $m = 1$ and $m = 0.01$ (not shown in the figure). It should also be noted that P is not constant on a fibre. For example, the P fibre shows in general a low stability but its stability is very high where it joins the B fibre (at the $\phi_1 = 0^\circ$, $\phi = 90^\circ$, $\phi_2 = 30^\circ$ position).

For the present selected set of reference stresses, the most stable is the B fibre followed by the P. The other fibres show little stability; along the Y fibre, even negative values

of P can occur. The value $P = 0.69$ when the plastic spin vanishes (i.e. when the lattice spin is equal to the rigid body spin (see Eq. (7)) is also indicated on Fig. 5 by the dotted lines. When P is higher than this value, the rotation rate of the grains is lower than the rigid body spin and vice versa. It is clear that in orientation regions where grains rotate nearly with the rigid body spin, significant orientation accumulations cannot happen, so the C_1 – C_2 , the Y and part of the P fibre are not expected to be significant in the development of the orientation distribution function (ODF) of Mg.

One can estimate the smallest possible P value from the lattice spin and the rigid body spin. A maximum value of the lattice spin can occur when the plastic spin is equal to the rigid body spin but opposite to it (see Eq. (7)). (This situation can be readily shown when single slip takes place in a grain for a specific orientation.) One then obtains: $P_{\min} = -0.549$.

In order to understand the behaviour of certain features of the evolution of the texture, it is useful to study the case in which an orientation just rotates with the rigid body spin under simple shear conditions. Such a case happens, for example, for simple shear of any rotated cube oriented grain (i.e. for which $\phi = 0^\circ$) with an fcc crystal structure [19]. According to Eq. (7), when the plastic spin is zero, the rate of lattice rotation is equal to the rigid body spin. For any orientation for a given imposed strain rate, the scalar rates of the rigid body $|\dot{\beta}|$ and lattice spins $|\dot{\omega}|$ can be defined as follows:

$$|\dot{\beta}| = \left(\dot{\beta}_{32}^2 + \dot{\beta}_{31}^2 + \dot{\beta}_{12}^2 \right)^{1/2}, \quad |\dot{\omega}| = \left(\dot{\omega}_{32}^2 + \dot{\omega}_{31}^2 + \dot{\omega}_{12}^2 \right)^{1/2}. \quad (14)$$

In the following, we are interested in finding the locations in Euler space where the plastic spin is small with respect to the rigid body spin; a ratio of 10 is considered:

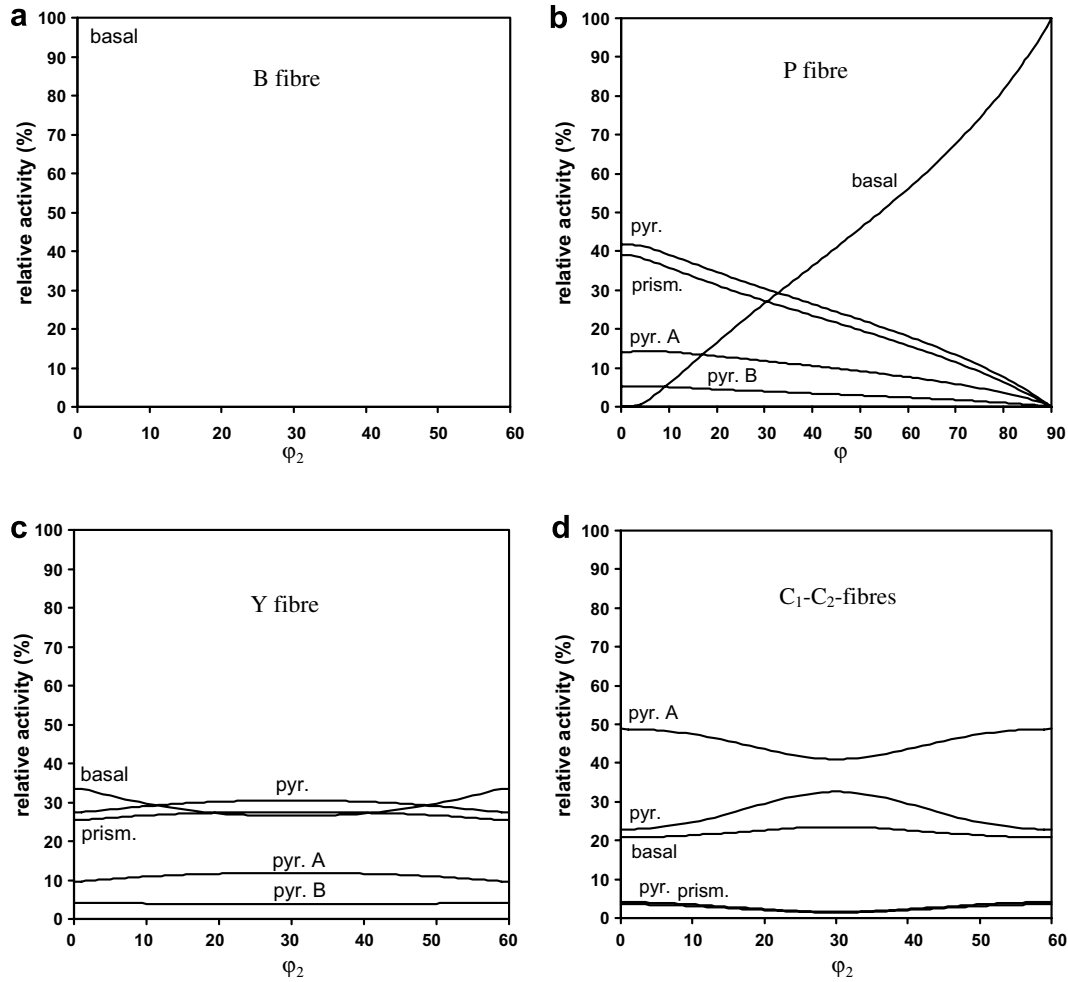


Fig. 4. Relative slip activities of the slip system families for the set of reference stresses [1, 8, 8, 6, 6], along: (a) B fibre, (b) P fibre, (c) Y fibre and (d) C₁-C₂ fibres.

$$|\dot{\omega}| = |\dot{\beta}|/10. \quad (15)$$

Fig. 6 shows the obtained result with the help of an iso-value-map in Euler space. Seven such fibres are identified: the β_1 fibre (15°, 0–15°, 0°), the β_2 fibre (45°, 75–90°, 0–60°), the β_3 fibre (135°, 75–90°, 0–60°), the β_4 fibre (30°, 82–90°, 0–60°), the β_5 fibre (60°, 82–90°, 0–60°), the β_6 fibre (120°, 82–90°, 0–60°), and the β_7 fibre (150°, 82–90°, 0–60°). As can be seen in Fig. 6, the plastic spin is not zero for any rotated $\varphi = 0^\circ$ orientation in the hcp crystals (the case which is equivalent to the rotated cube in fcc); it is so just for specific orientations, contrary to the case of the fcc structure.

4. Rotation field

In the preceding sections, we discussed the stability of a single crystal during plastic deformation. When a polycrystal is examined, many grains can be near the ideal orientations and the main question is the evolution of the orientation density $f(\mathbf{g})$ (i.e. the ODF). $f(\mathbf{g})$ depends mainly

on the characteristics of the rotation field in the vicinity of \mathbf{g} . The above analysis gave information about the velocity field $\dot{\mathbf{g}}$ using only a well-defined scalar quantity (P). Now, for a polycrystal, we are interested in the orientation flow in Euler space. For this purpose, the vector rotation field $\dot{\mathbf{g}} = (\dot{\varphi}_1, \dot{\varphi}_2)$ and the divergence quantity (Eq. (2)) have to be examined. These two quantities determine the evolution of the ODF given by the continuity equation of texture development [25,26]. In the ‘‘Lagrangian’’ formulation, when \mathbf{g} is not fixed, we have

$$\dot{f}/f + \dot{\varphi} \cot \varphi + \text{div}(\dot{\mathbf{g}}) = 0. \quad (16)$$

At a fixed point of Euler space (Eulerian description), the continuity equation becomes

$$(\dot{f}/f)_{\mathbf{g}} + \dot{\varphi} \cot \varphi + \text{div}(\dot{\mathbf{g}}) + \dot{\mathbf{g}} \text{grad}(\ln f) = 0. \quad (17)$$

Note that for $\dot{\mathbf{g}} = 0$ – the case of ideal orientations – Eqs. (16) and (17) are equivalent. The rate of change of the ODF intensity at a given orientation is characterized by $(\dot{f}/f)_{\mathbf{g}}$, which can be deduced from Eq. (17). For relatively weak textures, the term $\dot{\mathbf{g}} \text{grad}(\ln f)$ can be neglected for

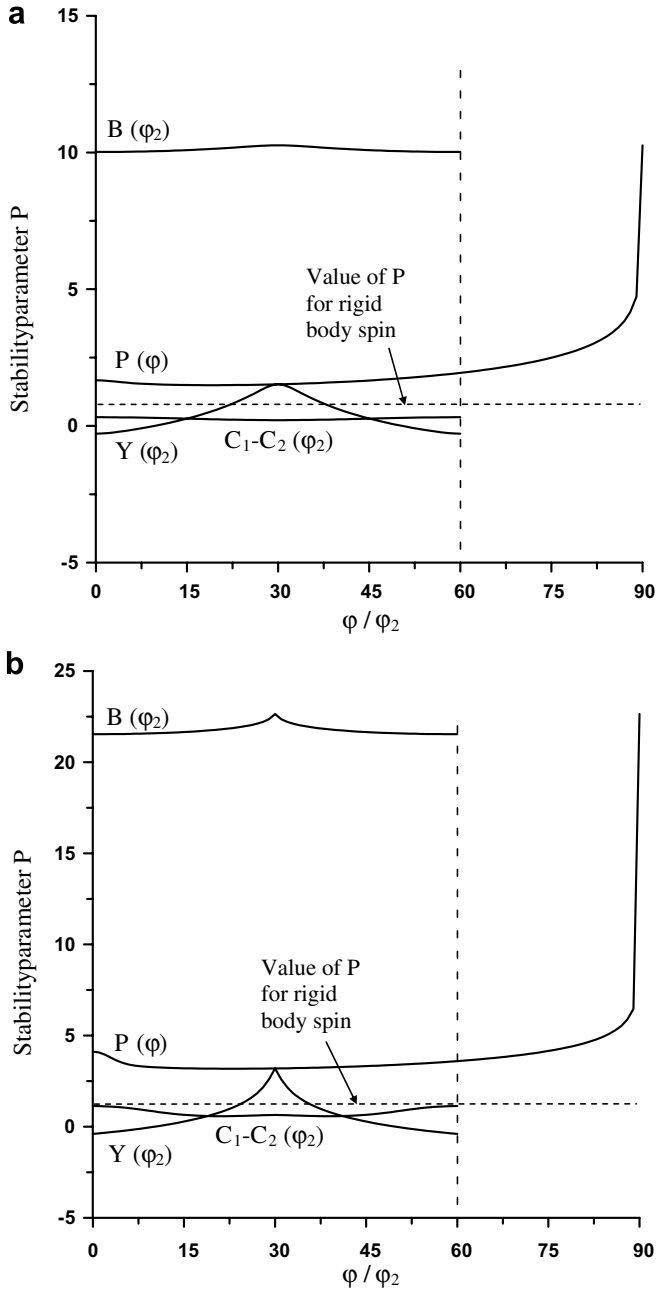


Fig. 5. The stability parameter P along the fibres for the crss set of [1, 8, 8, 6, 6] for two values of m : (a) 0.2 and (b) 0.1.

two reasons. First, \dot{g} is small near the ideal orientations; second, the $\text{grad}(\ln f)$ vector is also small if the texture is weak.

From the viewpoint of texture formation, a texture component at orientation g is considered to be stable during deformation as long as

$$\dot{g} = (\dot{\phi}_1, \dot{\phi}, \dot{\phi}_2) = 0 \quad \text{and} \quad (\dot{f}/f)_g > 0. \quad (18)$$

Fig. 7 shows both \dot{g} and $\text{div}(\dot{g})$ in four sections of the restraint Euler space; $\phi_2 = 0^\circ$, $\phi = 90^\circ$, $\phi_2 = 30^\circ$, and $\phi_1 = 0^\circ$. The divergence is calculated at grid points of Euler space separated by 1° , while the \dot{g} vector is on a grid of 5° . These four sections elucidate the characteristics around all

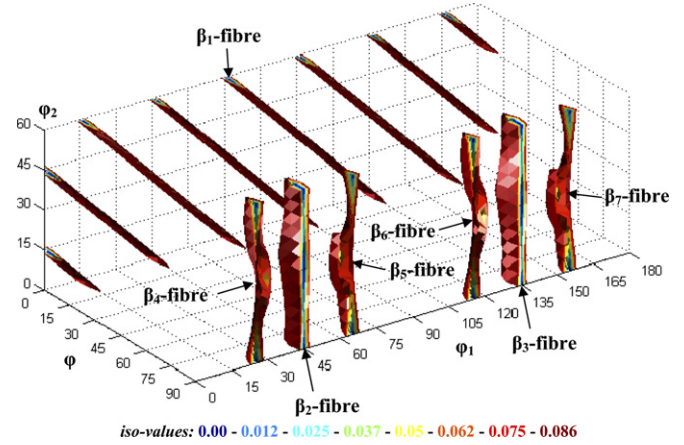


Fig. 6. Near-zero plastic spin locations in Euler space obtained for an applied rigid body rotation rate of 0.5 s^{-1} .

the fibres identified above. Blue regions represent the locations where $\text{div}(\dot{g}) < 0$, while the regions where $\text{div}(\dot{g}) > 0$ are identified by yellow and red. The arrows are the projections of the \dot{g} vectors in the sections of the Euler space considered. The relative reference stresses are [1, 8, 8, 6, 6], and m is 0.2.

In accordance with the definition of the orientation stability parameter (Eq. (11)), the rotation velocity \dot{g} shows a local minimum near the ideal orientations. \dot{g} is actually very small near the B and P fibres, meaning that these two fibres are the predominant ones during deformation. For all orientations, ϕ_1 is negative and significantly larger than $\|\dot{\phi}\|$ or $\|\dot{\phi}_2\|$. This means that the “global” movement of grains during simple deformation is a negative rotation around axis 3, i.e. rotation in the direction of shear. This rotation is represented by the Ω_{12} component of the lattice spin. When the plastic spin is small, the lattice rotation rate is $\Omega_{12} = 0.5 \text{ s}^{-1}$ for a shear rate of 1.0 s^{-1} . Assuming a hypothetical situation where this situation holds for large strains, the lattice rotation can accumulate up to 57.29° during a total simple shear of $\gamma = 2$.

Now the obtained results are analysed around the ideal fibres for positive simple shear using Fig. 7.

B Fibre: Grain orientations rotate towards the B fibre along the rotation vectors $-\vec{\phi}_1$ and $\vec{\phi}$; there is no orientation move along the $\vec{\phi}_2$ direction in the vicinity of the B fibre. The further an orientation is from the B fibre, the higher its rotation rate is.

P Fibre: Orientations rotate towards P along the rotation directions $-\vec{\phi}_1$ and $-\vec{\phi}_2$. Both the B and P fibres are located along a line $\text{div}(\dot{g}) = 0$. This is not the case for the Y fibre; it can be seen in Fig. 7d that the divergence is positive in the lower part ($0 \leq \phi_2 < 30^\circ$) and negative along its upper part ($30^\circ < \phi_2 \leq 60^\circ$). The rotation rate is also quite high. Similarly, the C_1 fibre is located in a zone where the divergence is negative, while the C_2 fibre is located in a positive divergence area (see Fig. 7b). For a negative shear direction, the situation is reversed for the C_1 and C_2 fibres. Considering the large

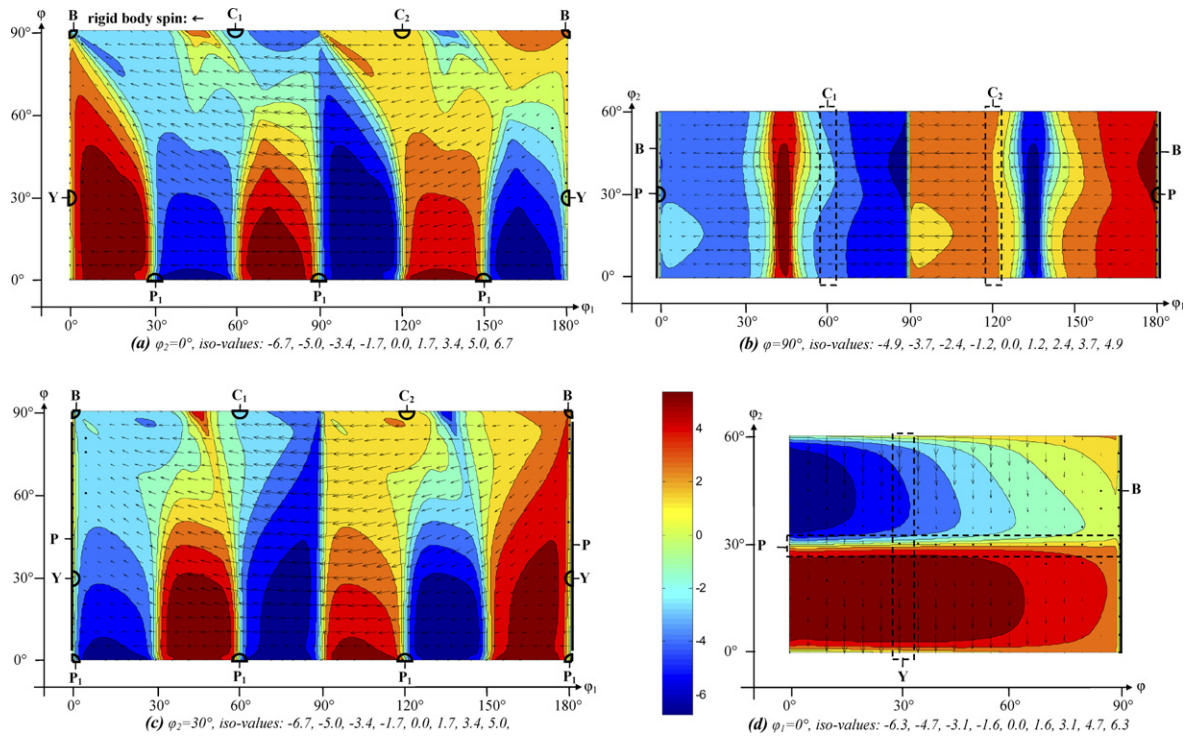


Fig. 7. Lattice rotation fields (\dot{g}) and divergences ($\text{div}(\dot{g})$) in the case of simple shear in the restraint Euler space. The relative reference stresses are [1, 8, 8, 6, 6] and the strain rate sensitivity is equal to 0.2. (a), (b), (c) and (d) correspond to sections $\phi_2 = 0^\circ$, $\phi = 90^\circ$, $\phi_2 = 30^\circ$ and $\phi_1 = 0^\circ$, respectively.

rotation vectors shown around these fibres compared to the B and P, together with the characteristics of the divergence, it can be again concluded that no significant ODF intensities would develop around the Y and C_1 – C_2 fibres in polycrystalline Mg.

5. Texture evolution in polycrystalline magnesium

The ideal orientations and the characteristics of the rotation field were identified in the preceding sections. The results of that analysis can be very helpful in the interpretation of the evolution of the crystallographic texture. For this purpose, two kinds of initial texture were considered: first a typical initial texture of an extruded Mg alloy, then a random distribution of grain orientations.

5.1. Experimental textures

Torsion tests were carried out on solid bar samples obtained from an extruded AZ71 bar (composition: 7 wt.% Al, 1 wt.% Zn, balance Mg) at 250 °C. The gauge length was 38 mm and the diameter of the bar was 6 mm. The torsion tests were conducted under ‘free-end’ conditions, i.e. with axial freedom of motion of the bars. A small amount of shortening (up to –2%) was recorded during torsion. The samples broke at a surface shear deformation of about 1.2. The initial as well as the deformation textures were measured by the orientation imaging (EBSD)

technique. The indexation quality was 80% in the non-deformed sample, while it was 40% in the deformed sample. This might appear to be a low indexation result, however, each grain was resolved. Moreover, further X-ray measurements have quantitatively confirmed the EBSD measurements. The texture in the deformed sample was measured by EBSD within a $500 \mu\text{m} \times 1500 \mu\text{m}$ surface parallel to the longitudinal axis of the sample in a zone where the average shear deformation was 0.9. The thus-obtained textures are presented in Fig. 8a and b in the form of pole figures where the projection is done on the r plane (r is the normal of the projection). As can be seen, the initial texture is a $\langle 10\bar{1}0 \rangle_z$ fibre texture with moderate strength. After a shear strain of 0.9, the texture is mainly rotated around the r axis in the direction of shear with an angle of about 30° . Some small intensity values are present near the C_1 and C_2 fibres; however, the intensity is less than random.

5.2. Texture modelling

5.2.1. Model parameters

The Taylor viscoplastic crystal plasticity model was used in which the textures were represented by 2000 crystal orientations. The relative reference stress values and the m -value were the same in the polycrystal model as in the rotation field analysis above, i.e. [1, 8, 8, 6, 6]. m is relatively high because the torsion tests were conducted at 250 °C [14]. Hardening was not considered in the simulations as the ratio of the maximum flow stress/yield

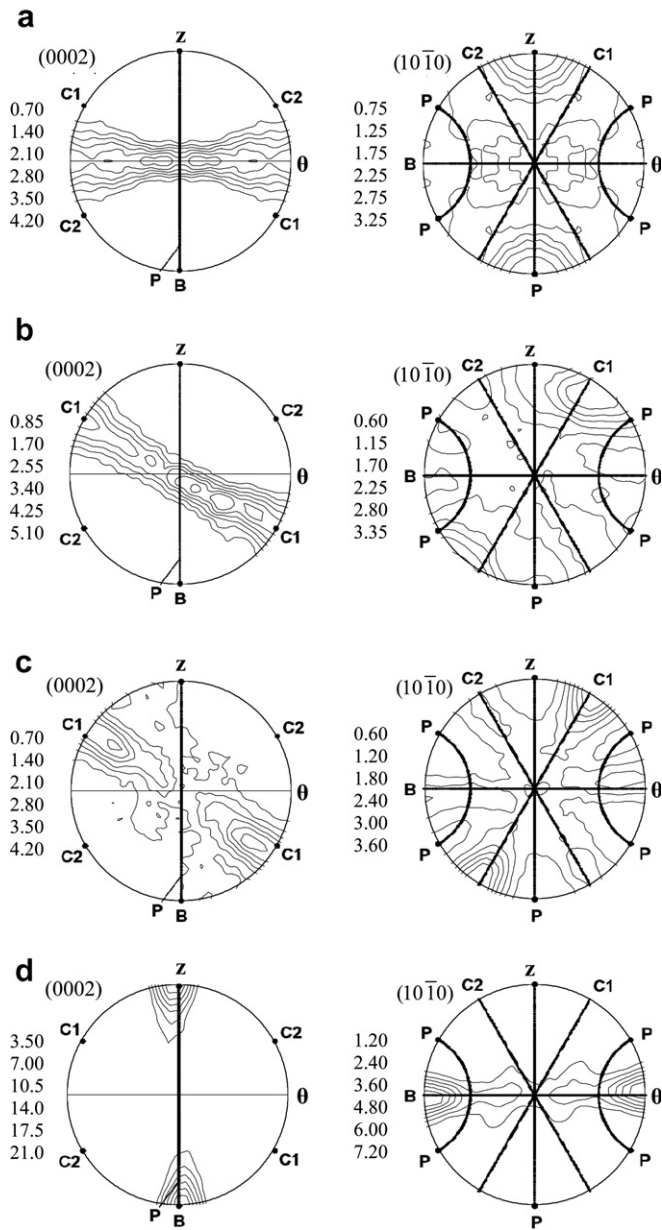


Fig. 8. Texture evolution during torsion of magnesium: (a) initial texture; (b) experimental texture, $\gamma = 0.9$; (c) simulated texture, $\gamma = 0.9$, [1, 8, 8, 6, 6] and (d) simulated texture, $\gamma = 4.0$, [1, 8, 8, 6, 6].

stress remained under 1.5 in the experiment, and there is not enough information available in the literature about hardening of this material to incorporate a suitable microscopic hardening law into the simulations (although numerically it would be readily possible). It is also true that the use of any kind of homothetic hardening law would not have any impact on the texture evolution as the Taylor model is used. The deformation of a material element in the torsion test was approximated by simple shear in the simulations in small increments (the shear acting in the z plane in the positive θ direction), i.e. the small axial strain was neglected (for simulation of the axial contraction, see Refs. [28,29]).

5.2.2. Texture development in torsion of the initially textured Mg bar

Fig. 8c shows the simulated texture at the same shear strain as the experiment ($\gamma = 0.9$). As can be seen, the main feature of the experimental texture, i.e. the rotation around the r axis, is qualitatively reproduced. The predicted rotation angle is 35° . If one compares this value to the rigid body rotation during the simple shear of 0.9, it is much less than that: 26° . At the same time, the experimental texture also seems to be rotated more than the rigid body rotation: by 30° . It is actually surprising that the overall rotation of the texture is more than the rigid body rotation.

In order to understand the large rotations observed above, the ODF of the initial texture is displayed in Fig. 9 in a 3-D presentation by showing the ODF from two views. As can be seen, the initial texture is such that all orientations are situated in the central part of the ODF. In these regions, however, the lattice rotation rate is high (see Fig. 7a and c). At many places, the lattice spin is even higher than the rigid body spin (the latter is indicated by an arrow above Fig. 7a). It is thus understandable

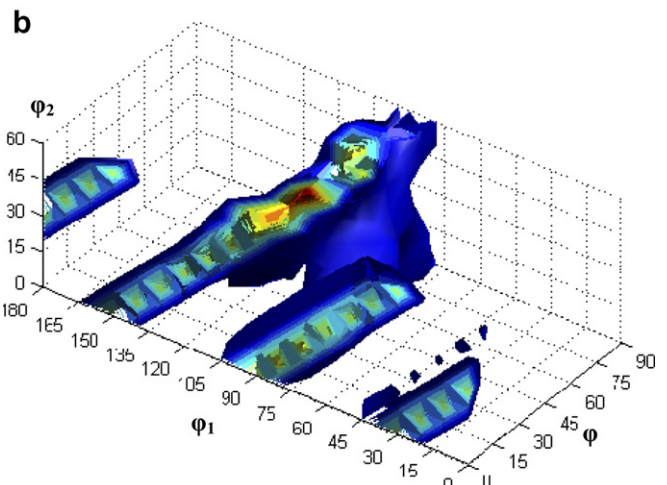
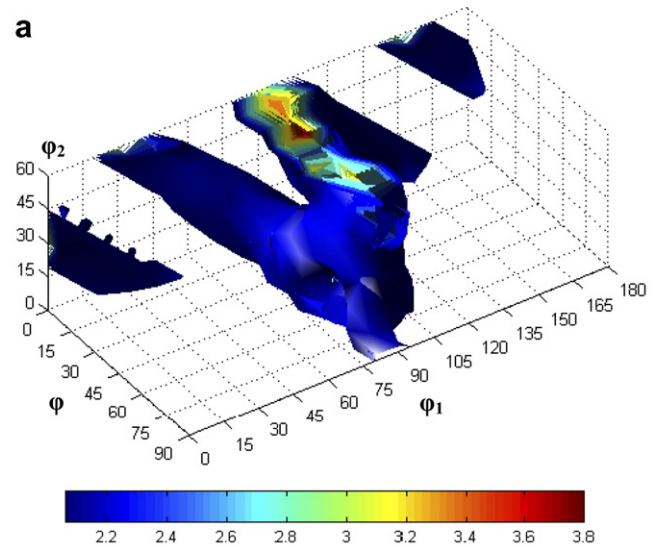


Fig. 9. The initial texture displayed in two views of the ODF.

that the accumulated experimental rotation of the texture is larger than the rigid rotation. Nevertheless, the strain is quite low (due to the limited plasticity of Mg in torsion), so the main ideal fibre (the B fibre) cannot be reached in a shear of 0.9. Even if the texture would rotate constantly by the rigid body rotation (which cannot be valid as the rotation of orientations approaching the ideal fibre slow down, see Fig. 4a and c), the strain needed would be $\gamma = 3.14$ (90° rotation). Such large strains can be reached by ECAE in multiple passes, and the interpretation of the corresponding simulations could be readily done using the above-presented stability maps and rotation field analysis. It can therefore be concluded that a general nearly rigid rotation of the texture takes place during a shear of 0.9 because of the nature of the initial texture and the rotation field.

At a large strain, $\gamma = 4$, the simulated texture in Fig. 8d shows that the B fibre appears, but in a slightly rotated position. More details about the evolution of the B fibre will be discussed in the following section.

5.2.3. Texture development in simple shear of an initially random texture in Mg

Two thousand orientations were used in the simulations with a random initial texture. Fig. 10 shows the obtained textures at increasing strains: $\gamma = 1.2, 2.1, 3.6$ and 8.1 in (0002) and $(10\bar{1}0)$ pole figures. The positions of the B, P and C_1 – C_2 ideal fibres are also indicated in the pole figures. For the relatively small strain, $\gamma = 1.2$, the B and C_1 – C_2 fibres are formed, the P fibre does not appear (and is absent even at larger strains). The presence of the C_1 and C_2 is surprising at first sight because it was found in the preceding section that these two fibres cannot be significant. Actually, they are not significant because their intensity is less than random. They are present mainly for the simple reason that the lattice rotation rate around them is nearly the same as the rigid body spin; thus, they represent a part of the initial random texture, which is simply rotated by the rigid body rotation. This particularity of the rotation field is very visible in Fig. 6, where the C_1 fibre is surrounded by the β_2, β_4 and β_5 , while the C_2 is located within the β_3, β_6 and β_7 fibres, which are the locations of nearly rigid body spin rotations. There are, nevertheless, some differences in intensities between the C_1 and C_2 fibres; the C_1 is stronger than C_2 . This can be explained with the help of the divergence map presented in Fig. 7, according to which the divergence is negative around C_1 but positive around C_2 .

With further straining, $\gamma = 2.1$, the C_1 – C_2 fibres weaken below the random value, while the B fibre persists with a non-uniform intensity distribution along the fibre. Finally, the C_1 – C_2 fibres completely disappear at $\gamma = 3.6$. Concerning the behaviour of the B fibre, it develops in a slightly rotated position with respect to its ideal position, opposite to the direction of shear. This “tilt” decreases as a function of strain and becomes positive at very large strains. At the same time, the intensity along the B fibre becomes more uniform.

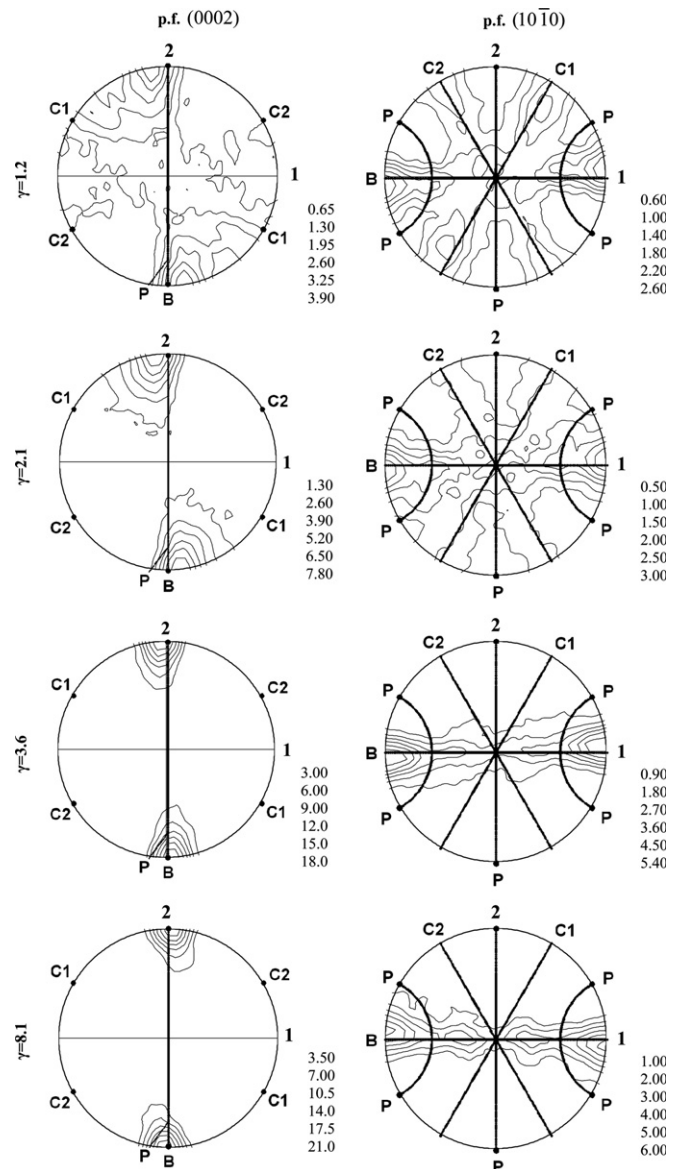


Fig. 10. Simulation of texture evolution during simple shear obtained by the viscoplastic Taylor model. Two thousand randomly oriented grains, reference stresses [1, 8, 8, 6, 6] and $m = 0.2$.

According to the above-presented texture development of an initially random texture, only the B fibre is important in polycrystalline Mg. The behaviour of the B can be analysed with the help of the rotation field characteristics presented in Sections 3 and 4 above. In a random initial texture, there are grain orientations everywhere, so orientations near B will approach the ideal position even at the onset of straining. However, they only approach from the right-hand side in the orientation space presented in Fig. 7a and c, coming from the negative divergence region. Therefore, they accumulate on the right side of the B ideal fibre in the ODF. In the pole figure, that position corresponds to the left side of the ideal fibre, so the B fibre component appears in slightly rotated position opposite to the applied shear. This “tilt” is about 7° at $\gamma = 1.2$ in Fig. 10 and decreases as a function of shear. The tilt even becomes

positive (i.e. in the sense of shear) at very large strains. Similar results were obtained in Ref. [30] for an initially random texture in simple shear for various values of m for another set of reference stresses [1, 2, 2, 3, 3].

It should be noted here that the positive tilt is an effect of the strain rate sensitivity of slip as it reduces as the strain rate sensitivity index m is decreased (see Ref. [30]). If one extrapolates to $m = 0$, the positive tilt does not appear at all. This tilt is possible because of the non-zero rotation of the grains even in the ideal position. As is shown in Fig. 5, the stability parameter P does not exceed 10 for the ideal positions when $m = 0.2$, so grain orientations can actually even cross the ideal position. It should be noted that the negative tilt develops also when m approaches zero because it is caused by the one-sided convergent nature of the rotation field, not by the large m value.

6. Conclusions

In the present work, the ideal positions of textures that develop under simple shear deformation are examined for the hexagonal crystal structure. For this purpose, the so-called orientation persistence parameter was employed, which can be obtained from the simulated lattice spin. The rotation field and the divergence quantity were also examined in orientation space in order to understand the behaviour of the ideal orientations. Experimental results were presented for the torsion of polycrystalline Mg–7Al–Zn alloy; these were modelled with the help of the Taylor viscoplastic model. From the results obtained, the following conclusions can be made:

1. With the help of the persistence parameter P , all possible ideal orientations are identified for hexagonal crystal textures in simple shear. They are all fibers, which are named B, P, Y, C_1 and C_2 .
2. For the case of Mg, with the set of reference stress values [1, 8, 8, 6, 6], the orientation persistence was examined in Euler space. It was found that only the B fibre is significant in Mg.
3. Simulations for the texture development in an initially random texture using the Taylor viscoplastic model revealed tilts of the ideal fibres from their ideal positions in simple shear. These tilts are opposite to the shear (negative) at lower strain, and become positive at large strains. They are caused by the convergent/divergent nature of the rotation field around the ideal fibres and by the non-zero lattice spin, even in the ideal positions, due to the rate sensitivity of slip.

4. The experimental textures in simple shear of initially $\langle 10\bar{1}0 \rangle \| z$ textured Mg rotate slightly more than the rigid body rotation at a shear of 0.9 due to the specific rotation field in the initial texture. The simulation with the Taylor model also gives a higher rotation value of the texture with respect to the rigid body rotation.

Acknowledgements

This work was partially funded by the Natural Sciences and Engineering Research Council of Canada (NSERC). K.W.N. is Canada Research Chair in Advanced Engineered Material Systems and the support of this program is gratefully acknowledged. B.B. thanks the Consulat général de France à Québec and the Ministère des relations internationales québécois for their financial support.

References

- [1] Tóth LS, Gilormini P, Jonas JJ. Acta Metall 1988;3077:3091.
- [2] Bunge HJ. Z Metallkde 1965;872:874.
- [3] Tóth LS, Jonas JJ, Gilormini P, Bacroix B. Int J Plasticity 1990;83:10.
- [4] Tóth LS, Neale KW, Jonas JJ. Acta Metall 1989;2197:2210.
- [5] Tóth LS, Jonas JJ, Daniel D, Ray RK. Metall Trans 1990;2985:3000.
- [6] Zhou Y, Neale KW, Tóth LS. Acta Metall Mater 1992;2921:2930.
- [7] Baczynski J, Jonas JJ. Acta Mater 1996;4273:4288.
- [8] De Messemacker J, Verlinden B, Van Humbeeck J. Acta Mater 2005;4245:4257.
- [9] Yoshinaga H, Horiuchi R. Trans JIM 1963;134:141.
- [10] Roberts CS. Magnesium and its alloys. New York: Wiley; 1964.
- [11] Balasubramanian S, Anand L. Acta Mater 2002;133:148.
- [12] Agnew SR, Yoo MH, Tomé CN. Acta Mater 2001;4277:4289.
- [13] Agnew SR, Mehrotra P, Lillo TM, Stoica GM, Liaw PK. Mater Sci Eng A 2005;72:78.
- [14] Agnew SR, Mehrotra P, Lillo TM, Stoica GM, Liaw PK. Acta Mater 2005;3135:3146.
- [15] Agnew SR, Duygulu O. Int J Plasticity 2005;1161:1193.
- [16] Turner PA, Tomé CN. Acta Mater 1994;4143:4153.
- [17] Hutchinson JW. Proc Roy Soc London 1976;101:127.
- [18] Asaro RJ, Needleman A. Acta Metall 1985;923:953.
- [19] Tóth LS, Jonas JJ. Textures Microstruct 1989;195:209.
- [20] Neale KW, Tóth LS, Jonas JJ. Int J Plasticity 1990;45:61.
- [21] Van der Giessen E, Wu PD, Neale KW. Int J Plasticity 1992;773:801.
- [22] Havner KS. Proc Roy Soc London 1981;329:349.
- [23] Havner KS. Philos Trans Roy Soc London 1984;469:493.
- [24] Havner KS. On Hill's stress rate in the continuum mechanics of polycrystals. Acta Mech 1972;183:187.
- [25] Clement A. Coulomb P Scripta Metall 1979;13:899.
- [26] Gilormini P, Toth LS, Jonas JJ. Proc Roy Soc London 1990;489:507.
- [27] Gelfand L, Minlos RA, Shapiro ZYA. Representation of the rotation and Lorentz groups and their applications. Oxford: Pergamon Press; 1963.
- [28] Qods F. Ph.D. thesis, Université de Metz, France, 2006.
- [29] Qods F, Tóth LS, Kloeden B, Beausir, B. In: Sixth ESMC European solid mechanics conference, Budapest, CD.
- [30] Beausir B, Tóth LS, Neale KW. Int J Plasticity 2007;227:243.